PCCP

Accepted Manuscript

ROYAL SOCIETY OF CHEMISTRY

www.rsc.org/pccp

Chemical Original and Catalytic Activity of Coinage Metals: From Oxidation to Dehydrogenation

*Cih-Ying Syu, Hao-Wen Yang, Fu-Hsing Hsu, Jeng-Han Wang**

Department of Chemistry, National Taiwan Normal University, Taipei, 11677, Taiwan, R.O.C.

Corresponding Author

* Jeng-Han Wang, Electronic mail: jenghan@ntnu.edu.tw, Phone: +886-2-77346123

Abstract:

The high oxidation activity for coinage metals (Cu, Ag and Au) has been widely applied on various important reactions, such as oxidation of carbon monooxide, alkenes or alcohols. The catalytic behavior of those inert metals has mostly been attributable to their size effect, the physical effect. In the present study, the chemical effects on their high oxidation activity has been investigated. We mechanistically examine the direct and oxygenate dehydrogenation (partial oxidation) reactions of ethanol to acetaldehyde on a series of transition metals (Groups 9, 10 and 11) with identical physical characteristics and varied chemical origins using density functional theory (DFT) calculations and electronic structure analyses at the GGA-PW91 level. The energetic results show that coinage metals have much lower activation energies and higher exothermicities for the oxidative dehydrogenation steps although they have higher energy for the direct dehydrogenation reaction. In the electronic structure analyses, coinage metals with saturated d bands can efficiently donate electrons to O* and OH*, or other electronegative adspecies, and better promote their p bands to higher energetic levels. The negatively charged O* and OH* with high-lying p bands are responsible for lowering the energies in oxidative steps. The mechanistic understanding well explains the better oxidation activity for coinage metals and provides the valuable information for the utilization of them on other useful applications, for example, the dehydrogenation process.

KEYWORDS: Coinage metals, Dehydrogenation, Density functional calculations, Ethanol, Partial oxidation.

Introduction

Coinage metals have attracted tremendous attention due to their good reactivity for various important processes in the heterogeneous catalysis. The interest started from the discovery of CO oxidation on gold catalysts at low temperatures in the 1980s,[1] while the moderate catalytic activity of the chemically inert gold is attributable to the remarkable size effect in the nano scale. Recently, coinage-metal clusters supported on reducible oxides also show the high activities for the oxidation or oxidative coupling of alcohols and olefins, even for large clusters (> 15 nm), as summarized in the reviews.[2-4] Additionally, the extended surfaces of coinage metals display similar catalytic behavior in the ultrahigh vacuum (UHV) condition as well.[5-7] Those results demonstrate that the intrinsic chemistry of coinage metals also plays an essential role in their oxidation activity. Thus, finding the chemical origin of coinage metals will have a significant influence on the understanding of their catalytic behavior and guide the design of their future applications.

To elucidate the oxidation activity of coinage metals, we mechanistically examine the partial oxidation of ethanol to acetaldehyde, which is an important transformation for fine chemical synthesis and has the modest importance in both scientific understanding and engineering application. This reaction has been extensively investigated on coinage metals[2-4] and in various conditions, including the oxidative steam reforming (OSR) in the continuous flow system,[8-14] aerobic oxidation in the batch reactor[15-18] and electro-oxidation reaction in alkaline medium.[19-22] These experiments confirm that the catalysts of coinage-metal nanoparticles or clusters on oxide supporters have great oxidation capability. In both OSR and aerobic oxidation experiments, higher oxygen or steam contents can further enhance the conversion efficiency of ethanol and increase the selectivity for oxidative products.[11, 14] In electrochemical reactions, hydroxyl ion in the alkaline medium plays an important role in the oxidation reaction. Additionally, the reaction

mechanism has been extensively investigated by *in situ* IR spectroscopy in practical catalytic conditions,[8-9, 23] UHV system at low pressure on single crystal surfaces[5-6, 24-25] and density functional theory (DFT) calculations at the molecular level.[21, 26-29] The mechanistic studies conclude that the partial oxidation of ethanol to acetaldehyde corresponds to the oxidative dehydrogenation reaction. Surface oxygen (O*) or hydroxyl (OH*), acting as Brønsted base or nucleophilic groups, can promote the reaction by thermodynamically and kinetically assisting the initial O–H and the followed C_α–H bond cleavages of adsorbed ethanol (CH_3CH_2OH*) and ethoxy (CH_3CH_2O*), respectively. Some results suggest that coinage metals themselves can promote the C_α–H bond cleavage as well.[8-9, 21, 25, 29] Oxide supports, on the other hand, play a key role for the initial O* and OH* formation and are less significant in the following dehydrogenation process.[15, 21, 29] These intensified researches indeed prove that the coinage metals are active catalysts for oxidation reaction and reveal feasible reaction routes at the molecular level. However, most of studies only dedicate on the coinage metals themselves and no comparison results with other TMs have been thoroughly examined for the elucidation of their chemical effect on the oxidation reactivity.

In the present study, we systematically investigate the oxidation reaction on a series of chemically corresponded transition metals (TMs) in Groups 9 (Co, Rh, Ir), 10 (Ni, Pd, Pt) and 11 (Cu, Ag, Au) using DFT calculations at the GGA-PW91 level. The (111) facet, which is the most dominant configuration and can well represent the nature for close-packed TMs,[7] is applied to model these TM catalysts. The surface science study in the clean system (UHV condition for single-crystal materials) has shown good correspondence to the catalytic experiments under the practical conditions (metal clusters at the atmospheric pressure or in the liquid phase) for current oxidation reaction.[2, 5, 30] Thus, the computed reaction energy (ΔE) and activation barrier (*Ea*) in our DFT calculations can be appropriate applied to rationalize the experimental observation.

Furthermore, the energetics, density of state (DOS) and charge distribution are analyzed to investigate the electronic structures of coinage metals. These mechanistic results can well serve as the guidance in understanding the origins of the catalytic behavior and predicting of possible applications suitable for coinage metals.

Results and discussion

Adsorption energies, $E_{ads}(A^*) = E(A^*) - E(\text{surface}) - E(A_{(g)})$ (the total energies of the surface with adsorbed A*, clean surface and gas-phase A, respectively), of the intermediates involved in the dehydrogenation reaction for ethanol to acetaldehyde on the TM surfaces, Co(111), Ni(111), Cu(111), Rh(111), Pd(111), Ag(111), Ir(111), Pt(111) and Au(111), have been initially examined and listed in Table 1. The comparisons of E_{ads} on all TMs are shown in Fig. 1a. Top and side views of the corresponded structures on Au(111), for example, are shown in Figs. 1b and S1 (ESI), respectively. The adsorption structures on other TMs are similar, not shown here, implying that the energetic results are mainly affected by the chemical characteristics of those TMs and their physical effect is negligible. Comparing E_{ads} of the adspecies, the stable molecules of $CH_3CH_2OH^*$, CH_3CHO^* and H_2O^* (black bars in Fig. 1a) are weakly bonded to all surfaces, $E_{ads} < -0.5$ eV, while other intermediates of $CH_3CH_2O^*$, CH_3CHOH^*, OH^*, O^* and H^* (color bars in Fig. 1a) have much stronger adsorption energies. Comparing E_{ads} on the TM surfaces, the adsorption energy decreases as the adsorbed TMs move from left to right across the Periodic Table. On the other hand, coinage metals, which have filled d orbitals and are relatively inert, show the lowest adsorption energies for most adspecies.

The mechanism for the partial oxidation of ethanol to acetaldehyde corresponding to the dehydrogenation reaction of surface ethanol ($CH_3CH_2OH^*$) includes two parallel pathways. The

first pathway follows the O–H bond cleavage of $CH_3CH_2OH^*$ and C_α–H bond cleavages of $CH_3CH_2O^*$ in steps **f1** and **f2**, respectively.

$CH_3CH_2OH^* \rightarrow CH_3CH_2O^* + H^*$ (**f1**)

$CH_3CH_2O^* \rightarrow CH_3CHO^* + H^*$ (**f2**)

The second pathway, with an opposite order, follows the C_α–H bond cleavage of $CH_3CH_2OH^*$ and O–H bond cleavage of CH_3CHOH^* in steps **s1** and **s2**, respectively.

$CH_3CH_2OH^* \rightarrow CH_3CHOH^* + H^*$ (**s1**)

$CH_3CHOH^* \rightarrow CH_3CHO^* + H^*$ (**s2**)

On clean TM surfaces, those four steps (denoted as $\mathbf{M_x}$, **x** = **f1**, **f2**, **s1** and **s2**) are related to the direct dehydrogenation reaction. In the steam reforming and electrochemical experiments, the reducible oxide supporters and alkaline medium can create O* and OH* on the TM surfaces. When those steps occur on O* and OH* adsorbed TM surfaces, the dissociated H from ethanol or its fragments can bond with O* and OH* (denoted as $\mathbf{O_x}$ and $\mathbf{OH_x}$, respectively) in the oxidative dehydrogenation reactions, also known as partial oxidation. The four steps on the clean, O* and OH* adsorbed TM surfaces have been systematically investigated on the identical (111) surface for those TMs to elucidate the catalytic mechanism in the reforming and electro-oxidation experiments. The DFT computed ΔE and *Ea* are listed in Table 2. Top and side views of the related structures of local minimums and transition states on Au(111), for example, are shown in Figs. 2 and S2, respectively. The optimized structures on other TM surfaces are similar and not shown. The alike structures on the TM surfaces also imply that the energetic results mainly correspond to the chemical effect of those TMs. Also, those energies are initially examined with Brønsted–Evans–Polanyi (BEP) relation, as shown in Fig. S3 (ESI), to validate the computational consistence. Good BEP correlations (the coefficient $R^2 > 0.93$) between *Ea* and ΔE of all steps on those TM surfaces are obtained.

Shown in Fig. 3a is the overall *E* comparison for all the 12 steps, $\mathbf{M_x}$, $\mathbf{O_x}$ and $\mathbf{OH_x}$ (x = **f1**, **f2**, **s1** and **s2**), on the nine TM surfaces, Groups 9 (Co, Rh, Ir) in black open symbols, 10 (Ni, Pd, Pt) in blue open symbols and 11 (Cu, Ag, Au) in red filled symbols. Comparing steps **f1**, **f2**, **s1** and **s2**, *Ea* ranges for both C_α–H bond cleavages (steps **f2** and **s1**) are higher than those for the two O–H bond cleavages (steps **f1** and **s2**). C_α–H bond cleavage for CH_3CH_2OH* (step **s1**) shows the highest *Ea* in the range of 0.81 – 2.52 eV, suggesting that CH_3CH_2OH* energetically prefers the first pathway (CH_3CH_2OH* → CH_3CH_2O* → CH_3CHO*) on the TM surfaces. Also, *Ea* range for the first O–H bond cleavage (step **f1**) is relatively lower than that for the followed C_α–H bond cleavage (step **f2**), implying that CH_3CH_2O* is abundant on the surface and has sufficient lifetime to be observed in the experiments for ethanol catalytic reactions.[5-6, 8-9, 23-25]

Comparing $\mathbf{M_x}$, $\mathbf{O_x}$ and $\mathbf{OH_x}$ steps, the *Ea* ranges for O* and OH* assisted bond cleavages ($\mathbf{O_x}$ and $\mathbf{OH_x}$ steps) are relatively lower than those for direct bond cleavage ($\mathbf{M_x}$ step). This result indicates that O* or OH* can efficiently improve the dehydrogenation reaction and agrees with the experimental observation that higher steam or oxygen contents show better catalytic efficiency as described in Introduction. Comparing the energies on those TM surfaces, coinage metals (red filled symbols) show the highest *Ea* for the direct dehydrogenation reaction in $\mathbf{M_x}$ steps. The higher barriers in $\mathbf{M_x}$ steps on coinage metals are attributable to the weaker E_{ads} of the related adspecies, which have less effect on weakening the intramolecular bonding of adspecies and lowering the *Ea*.[31-33] On the other hand, coinage metals show the lowest *Ea* for the oxidative dehydrogenation reaction in $\mathbf{O_x}$ and $\mathbf{OH_x}$ steps. The lower *Ea* on Cu(111), Ag(111) and Au(111) in $\mathbf{O_{f1}}$ (0.19, 0.13 and 0.25 eV) and $\mathbf{OH_{f1}}$ (0.18, 0.08 and 0.05 eV) steps than in $\mathbf{M_{f1}}$ (0.77, 1.04 and 1.13 eV) steps are consistent with the experimental observation that O*[5-7, 9, 24-25, 30] and OH*[19, 21-22] on coinage metals can fasten the production of surface ethoxy. The lower *Ea* on Cu(111), Ag(111) and Au(111) in $\mathbf{O_{f2}}$ (1.05, 0.66 and 0.57 eV) and $\mathbf{OH_{f2}}$ (0.82, 0.49 and 0.37 eV)

steps than in $\mathbf{M_{f2}}$ (1.64, 1.46 and 1.20 eV) steps also clarify that C_α–H bond cleavage is not promoted by coinage metals themselves, but their surface O* and OH*.

The influences from O* and OH* on all TM surface have been further detailed by examining the *Ea* differences, [*Ea*($\mathbf{O_x}$)–*Ea*($\mathbf{M_x}$)] (red bars) and [*Ea*($\mathbf{OH_x}$)–*Ea*($\mathbf{M_x}$)] (blue bars), between the oxidative and direct dehydrogenation reactions. Shown in Figs. 3b and 3c are the *Ea* differences for steps **f1** and **f2** in the energetically preferred first pathway. The *Ea* differences for steps s1 and **s2** in the second pathway are shown in the Fig. S4 (ESI). All the four steps show a similar energetic trend that most TMs have negative *Ea* differences and coinage metals have the largest one. This result implies that O* and OH* can boost the dehydrogenation reactions, especially on coinage metals. The less negative or some positive *Ea* differences are observed for the TMs in the left d block, such as Co, Ni and Rh, indicating that O* and OH* will retard the dehydrogenation reaction on those TMs. This result also implies that the activity of O* and OH* decreases as the adsorbed TMs move from right to left across the Periodic Table. Similar trend is also observed for the O–H bond cleavage of surface water in previous study.[34-35] Thus, the main differences between coinage metals and other TMs corresponds to the largest *Ea* drop from direct to oxidative dehydrogenation reactions. This energetic drop is attributable to their highly active O* and OH* and responsible for their high oxidation activity in the reforming and electro-oxidation experiments. Additionally, significant energetic drops are also found on (100), (110) and (211) surfaces of coinage metals, shown in Table S1 and Fig. S5 (ESI), indicating that the energetic behavior and oxidation activity on coinage metals are insensitive to their surface structures and mainly correspond to their chemical origins. Furthermore, the chemical effects of how O* and OH* are highly active on coinage metals or how coinage metals can effectively activate O* and OH* have been elucidated in the following adsorption/desorption energy, binding energy, density of state (DOS) and charge distribution analyses.

Dehydrogenation steps on the clean, O* and OH* adsorbed TM surfaces ($\mathbf{M_x}$, $\mathbf{O_x}$ and $\mathbf{OH_x}$, respectively) can be expressed as follows.

$A^* \rightarrow B^* + H^*$ ($\mathbf{M_x}$)

$A^* + O^* \rightarrow B^* + OH^*$ ($\mathbf{O_x}$)

$A^* + OH^* \rightarrow B^* + H_2O^*$ ($\mathbf{OH_x}$)

A* and B* are exactly the same for those steps on the clean, O* and OH* adsorbed surfaces. For example, A* and B* are $CH_3CH_2OH^*$ and $CH_3CH_2O^*$, respectively, in step **s1** and are $CH_3CH_2O^*$ and CH_3CHO^*, respectively, in step **s2**. Due to the small adsorbate effects (Table S2, ESI), the reaction energies of $\Delta E(\mathbf{M_x})$, $\Delta E(\mathbf{O_x})$ and $\Delta E(\mathbf{OH_x})$ for those dehydrogenation steps can be fairly represented as the energies for reactant desorption, product adsorption and intermediate reaction in the gas phase as rearranging in the following equations:

$$\Delta E(\mathbf{M_x}) = [E_{ads}(B^*) - E_{ads}(A^*)] + [E_{ads}(H^*)] + [E(B_{(g)}) - E(A_{(g)}) + E(H_{(g)})]$$

$$\Delta E(\mathbf{O_x}) = [E_{ads}(B^*) - E_{ads}(A^*)] + [E_{ads}(OH^*) - E_{ads}(O^*)] + [E(B_{(g)}) - E(A_{(g)}) + E(OH_{(g)}) - E(O_{(g)})]$$

$$\Delta E(\mathbf{OH_x}) = [E_{ads}(B^*) - E_{ads}(A^*)] + [E_{ads}(H_2O^*) - E_{ads}(OH^*)] + [E(B_{(g)}) - E(A_{(g)}) + E(H_2O_{(g)}) - E(OH_{(g)})]$$

The energies for gas-phase reactions in the third brackets are irrelevant to the TM surfaces, indicating that the ΔE trend only corresponds to product desorption and reactant adsorption energies in the first two brackets. Furthermore, the first brackets $[E_{ads}(B^*) - E_{ads}(A^*)]$, related to A* desorption and B* adsorption energies, are exactly the same in the three ΔE representations. Thus, only the second brackets of $[E_{ads}(H^*)]$, $[E_{ads}(OH^*) - E_{ads}(O^*)]$ and $[E_{ads}(H_2O^*) - E_{ads}(OH^*)]$ directly correspond to the trends of $\Delta E(\mathbf{M_x})$, $\Delta E(\mathbf{O_x})$ and $\Delta E(\mathbf{OH_x})$, respectively, on the TMs.

Eventually, they correspond to the trends of $Ea(\mathbf{M_x})$, $Ea(\mathbf{O_x})$ and $Ea(\mathbf{OH_x})$ because of the good BEP correlations.

Coinage metals have less exothermic E_{ads}(H*) and result the higher $\Delta E(\mathbf{M_x})$ and $Ea(\mathbf{M_x})$. [E_{ads}(OH*)–E_{ads}(O*)] mainly follows the trend of –E_{ads}(O*) since E_{ads}(O*) is much larger than E_{ads}(OH*). Coinage metals have smallest –E_{ads}(O*) and results the lowest $\Delta E(\mathbf{O_x})$ and $Ea(\mathbf{O_x})$. Similarly, the trend of [E_{ads}(H_2O*)–E_{ads}(OH*)] follows that of –E_{ads}(OH*) as E_{ads}(H_2O*) is negligible. Coinage metals have the smallest –E_{ads}(OH*) and result the lowest $\Delta E(\mathbf{OH_x})$ and $Ea(\mathbf{OH_x})$ as well. $Ea(\mathbf{O_x})$ and $Ea(\mathbf{OH_x})$ have opposite trends to that of $Ea(\mathbf{M_x})$ since the trends of –E_{ads}(O*) and –E_{ads}(OH*) are opposite to that of E_{ads}(H*). Those results explain the *Ea* behavior of coinage metals in Fig 3a (red filled symbols). Additionally, the *Ea* differences of [$Ea(\mathbf{O_x})$–$Ea(\mathbf{M_x})$] and [$Ea(\mathbf{OH_x})$–$Ea(\mathbf{M_x})$] in Figs. 3b and 3c are proportional to the E_{ads} differences, [E_{ads}(OH*)–E_{ads}(O*)]–[E_{ads}(H*)] (red bars) and [E_{ads}(H_2O*)–E_{ads}(OH*)]–[E_{ads}(H*)] (blue bars), respectively, in Fig. 4a. Coinage metals have the smaller E_{ads} differences, give the larger *Ea* drop and ultimately show the higher oxidation activity.

The adsorption/desorption energy analysis finds that the *Ea* trend of partial oxidation reaction of ethanol to acetaldehyde corresponds to –E_{ads}(O*) and –E_{ads}(OH*); however, the energetics of other adspecies (CH_3CH_2OH*, CH_3CH_2O*, CH_3CHOH* or CH_3CHO*) are less significant. On the other hand, coinage metals with filled d orbitals have the lowest –E_{ads}(O*) and –E_{ads}(OH*) and the highest activated O* and OH* to assist the oxidation reaction. This result also implies that coinage metals can promote other catalytic reactions in which O* or OH* is involved and is also supported by the experimental observation that coinage metals also shows better catalytic performance for CO oxidation[7, 36-40] and water-gas-shift reaction (WGSR).[31, 41-46]

The highly activated O* and OH* on coinage metals can also be verified from the binding energies of H to O* and OH* (denoted E_{bind}^{O*}(H) and E_{bind}^{OH*}(H), respectively), which

correspond to the exothermicities or stabilities when the dissociated H bonds to surface O* and OH*, respectively.

$$E_{bind}^{O*}(\mathrm{H}) = E(\mathrm{OH*}) - E(\mathrm{O*}) - E(\mathrm{H_{(g)}})$$

$$E_{bind}^{OH*}(\mathrm{H}) = E(\mathrm{H_2O*}) - E(\mathrm{OH*}) - E(\mathrm{H_{(g)}})$$

E(OH*), E(O*), E(H_2O*) and E($H_{(g)}$) are related to the total energies of the surfaces with adsorbed OH*, O*, H_2O* and gas-phase H atom, respectively. Referring binding energies to E_{ads}(H*), the energetic differences of [E_{bind}^{O*}(H) –E_{ads}(H*)] (red bars) and [E_{bind}^{OH*}(H) –E_{ads}(H*)] (blue bars) on the TMs are shown in Fig 4b. Positive energetic differences indicate the TM surfaces can better stabilize the dissociated H. For examples, positive ones are found on Co, Ni and Rh, suggesting that O* and OH* on those TMs will hinder the dehydrogenation reaction. On the other hand, negative energetic differences imply that O* and OH* are more active and can more tightly bind with the dissociated H. Coinage metals all have the negative ones, confirming that O* and OH* on their surfaces can better stabilize the dissociated H and have larger *Ea* drop in Figs. 3b and c. In addition, their largest negative values reveal that $\mathbf{O_x}$ and $\mathbf{OH_x}$ steps on coinage metals have the lowest *Ea* in the dehydrogenation reactions on all the TMs. Thus, O* or OH* covered coinage metals can be considered as the best catalysts for the dehydrogenation process.

It is noting that the trend of O* activity is slightly different from that of OH*. O* on coinage metals always shows highest activity; however, OH* on Cu somewhat has lower activity than on Pd, Ir and Pt, attributable to the more exothermic E_{ads}(OH*) on Cu. This result corresponds to the fact that Pd or Pt-based electrodes also show good performance in electro-oxidation experiments as well.

Those energetic analyses in Fig. 4 concludes that O* or OH* activities can be interpreted from their adsorption/desorption and binding energies. The smaller the E_{ads}(O*) and E_{ads}(OH*) are, the higher activities are O* and OH*. The more exothermic E_{bind}^{O*}(H) and E_{bind}^{OH*}(H) result higher O* and OH* activities as well. Furthermore, how O* and OH* are activated by coinage metals has been investigated by the electronic analysis of the TMs.

The DOS for O* and OH* on all the TM surfaces are analyzed for the understanding of electronic structures of bare, O* and OH* adsorbed TMs. Since Co and Ni are ferromagnetic, both spins α and β are included in the DOS analysis, as shown in Fig. 5. All the TM d bands and O p bands are marked in blue and red lines, respectively. The d bands for bare, O* and OH* adsorbed TM are marked in solid, dot and dash blue lines, respectively. The p bands for free $O_{(g)}$ and $OH_{(g)}$, which are the same for all TMs, are marked in thick and thin solid red lines, respectively, in the Co (upper-left) cell; the p bands for O* and OH* on TM surfaces are marked in dot and dash lines, respectively.

In the DOS analysis, all TM d bands have limited change while O p bands show dramatic change upon O* and OH* adsorptions. This result indicates that TM atoms on the clean, O* and OH* adsorbed surfaces have a similar catalytic activity and implies that the high oxidation activity of coinage metals mainly corresponds to the activated O* and OH*. Additionally, the analysis shows that the p bands of O* and OH* on coinage metals are quite different from those on other TMs.

When O* or OH* adsorbs on the surfaces, TM d band and O p band convert to bonding and antibonding bands for TM–O bond formation,[47] which locate at the lower (c.a. -6 eV) and higher (the Fermi level) energetic regions, respectively. Due to the filled d orbitals, coinage metals have lower energetic d bands (than O p band) that contribute mostly to the bonding band at the lower energy. Consequently, O* and OH* p bands mainly contribute to the antibonding bands at the

higher energy, as shown in small red bumps around the Fermi level. The high-lying p bands of O* and OH* are more active and can tightly bond with the dissociated H atom to show the largest *Ea* drop from $\mathbf{M_x}$ to $\mathbf{O_x}$ and $\mathbf{OH_x}$ steps on Cu(111), Ag(111) and Au(111) in Fig. 3. In opposite, d bands of unfilled TMs, such as Co, Ni and Rh, are energetically higher and contribute mostly to the antibonding bands; hence, their TM surfaces are more active to the dissociated H atom and those TMs favor direct dehydrogenation reaction.

The activity comparisons for O* and OH* on those TMs are also examined by the charge analysis. Shown in Fig. 6 are the side and top views of induced charge distributions upon O* adsorption on all the TMs. Positively and negatively induced charge distributions are marked in blue and red isosurfaces, respectively. The charge analyses for OH* on all the TMs, which are similar to those of O*, are shown in Fig. S6 (ESI).

The induced charges on coinage metals are quite different from those on other TMs. On Cu(111), Ag(111) and Au(111) surfaces, O* and OH* adsorptions induce less charge (either positive nor negative ones) on the metal–O* interface, corresponding to the weaker E_{ads}(O*) and E_{ads}(OH*) on them, while more negative charges are located on O* or OH* (the large red lobes). On the other hand, those d-band saturated coinage metals can be good electron donors in bonding with electronegative O* and OH*.[22, 38] The negatively charged O* and OH* are highly active that gives more exothermic E_{bind}^{O*}(H) and E_{bind}^{OH*}(H), lower ΔE and *Ea* in $\mathbf{O_x}$ and $\mathbf{OH_x}$ steps and, eventually, better oxidation activity. This observations also agree with previous studies that negatively charged O*[5, 27, 48] and OH*[19, 21-22] play important roles in the ethanol oxidation reaction on coinage metals. In contrary, more charges (both positively and negatively ones) are induced on the TM–O interfaces when O* adsorbs on d-band unfilled TMs. The denser charges on the interface reflect to the stronger E_{ads}(O*) on those TMs and induce less charges to O* and

OH*, which are less active. Thus, smaller *Ea* differences are found in $\mathbf{M_x}$, $\mathbf{O_x}$ and $\mathbf{OH_x}$ steps on those TMs (Fig. 3).

Conclusions

In conclusion, bare coinage metals with filled d orbitals are rather inert for the direct ethanol dehydrogenation reaction. Alternatively, adding O* or OH* on their surfaces can dramatically enhance their catalytic activity and give the best catalysts for the oxidative dehydrogenation reaction. The excellent oxidation activity for coinage metals originates from the highly activated O* or OH* with the highest exothermicities of $E_{bind}^{O*}(\mathrm{H})$ and $E_{bind}^{OH*}(\mathrm{H})$. The highly activated O* and OH* are attributable to their high-lying p bands and dense negative charges. The high-lying p bands of O* or OH* occur when coinage metal d bands distribute energetically lower than O or OH p bands. The dense negative charges correspond to that coinage metals can better induce electrons to electronegative adspecies. Based on the revealed mechanism, similar catalytic behaviors are also expected for the oxidation of other alcohols; for example, methanol,[22] 2-butanol,[49] cyclohexanol,[50] 2-cyclohexen-1-ol[51] and more complicated ones[52-54] can be easily oxidized on coinage metals as well. Additionally, the strong interaction between the dissociated H atom and surface O* or OH* on coinage metals should also assist the dehydrogenation reactions for other chemicals; for example, O* pre-covered coinage metals can efficiently dehydrogenate H_2O,[55] CH_2CHCHO,[56] CH_3O,[55] H_2COO,[55] CH_4,[57] NH_3[55, 58] and $CH_3(CH_2)_2NH_2$[59] in previous studies. Finally, our mechanistic result further suggests that pre-treating other electronegative adspecies, such as sulfur, nitrogen, halogens or carbon monoxide, on coinage metals can dramatically improve their catalytic activity from oxidation to dehydrogenation reactions and the enhanced activity will be the highest, higher than any pure TM catalysts.

Computational methods

The calculations were performed at the density functional theory (DFT) level with a 3D periodic boundary condition using the Vienna Ab initio Simulation Package (VASP).[60-62] The exchange-correlation function was utilized by generalized gradient approximation[63] with Perdew-Wang 1991 formulation,[64] known as GGA-PW91. The basis planewaves with kinetic energies below 600 eV (cutoff energy) were included in the calculation. The ion-core interactions were treated by the cost-effective pseudopotentials with projector-augmented wave method (PAW),[65-66] The Monkhorst-Pack scheme[67] for the special k-point sampling at 0.05 × 2 (1/Å) interval was applied to the Brillouin-Zone (BZ) integration in the reciprocal space. The spin polarized calculation was employed in the case of ferromagnetic Co, Ni and all gas-phase species.

The most stable (111) surface, which has been widely applied in the study of heterogeneous catalytic reactions on the close-packed TMs, was applied in the present calculation. The surface was constructed by a five-layer metal slab, each layer with a 4 × 4 surface unit, and an equivalent five-layer vacuum space to limit the artificial interaction between the distinct slabs. The bottom two layers of the modeled surface were fixed at the computed lattice constants to represent the semi-infinite bulk crystal and the top three layers were free to relax in the structure optimization. Structures were geometry-optimized to local-minima on their respective potential energy hypersurfaces by quasi-Newton method with an energetic convergence of 1×10^{-4} eV and a gradient convergence of 1×10^{-2} eV. Transition states of surface reactions were located by Nudged Elastic Band (NEB) method[68] at the same convergence criterions. Density of state (DOS) and charge distribution were analyzed in the optimized structures.

Acknowledgements

This work is supported by the National Science Council, Taiwan (NSC 101-2113-M-003-006). CPU time at Taiwan's National Center for High-performance Computing (NCHC) and Department of Applied Chemistry in Private Chinese Culture University (PCCU) is greatly appreciated.

Footnotes

Electronic supplementary information (ESI) available: Side views of adsorption structures, local minimums and transition states, details of the BEP correlations, *Ea* differences in steps **s1** and **s2**, adsorbate effect, and charge analyses of OH* on the TMs are included in ESI.

References

1. M. Haruta, T. Kobayashi, H. Sano and N. Yamada, *Chem. Lett.*, 1987, 405-408.
2. X. Liu, R. J. Madix and C. M. Friend, *Chem. Soc. Rev.*, 2008, **37**, 2243-2261.
3. B. K. Min and C. M. Friend, *Chem. Rev.*, 2007, **107**, 2709-2724.
4. S. E. Davis, M. S. Ide and R. J. Davis, *Green Chem.*, 2013, **15**, 17-45.
5. J. Gong and C. B. Mullins, *J. Am. Chem. Soc.*, 2008, **130**, 16458-16459.
6. I. E. Wachs and R. J. Madix, *Appl. Surf. Sci.*, 1978, **1**, 303-328.
7. J. Gong and C. B. Mullins, *Acc. Chem. Res.*, 2009, **42**, 1063-1073.
8. P.-Y. Sheng, G. A. Bowmaker and H. Idriss, *Appl. Catal. A*, 2004, **261**, 171-181.
9. Y. Guan and E. J. M. Hensen, *Appl. Catal. A*, 2009, **361**, 49-56.
10. B. M. Abu-Zied, *Appl. Catal. A*, 2000, **198**, 139-153.
11. C. P. Rodrigues, V. T. da Silva and M. Schmal, *Catal. Comm.*, 2009, **10**, 1697-1701.
12. J. Chen, X. Tang, J. Liu, E. Zhan, J. Li, X. Huang and W. Shen, *Chem. Mater.*, 2007, **19**, 4292-4299.
13. V. I. Sobolev, K. Y. Koltunov, O. A. Simakova, A.-R. Leino and D. Y. Murzin, *Appl. Catal. A*, 2012, **433-434**, 88-95.
14. C.-C. Hung, S.-L. Chen, Y.-K. Liao, C.-H. Chen and J.-H. Wang, *Int. J. Hydrogen Energy*, 2012, **37**, 4955-4966.
15. B. Jørgensen, S. E. Christiansen, M. L. D. Thomsen and C. H. Christensen, *J. Catal.*, 2007, **251**, 323-327.
16. K.-Q. Sun, S.-W. Luo, N. Xu and B.-Q. Xu, *Catal. Lett.*, 2008, **124**, 238-242.

17. C. H. Christensen, B. Jørgensen, J. Rass-Hansen, K. Egeblad, R. Madsen, S. K. Klitgaard, S. M. Hansen, Mike R. Hansen, H. C. Andersen and A. Riisager, *Angew. Chem. Int. Ed.*, 2006, **45**, 4648-4651.
18. H. Rajesht and U. S. Ozkan, *Ind. Eng. Chem. Res.*, 1993, **32**, 1622-1630.
19. Y. Kwon, S. C. S. Lai, P. Rodriguez and M. T. M. Koper, *J. Am. Chem. Soc.*, 2011, **133**, 6914-6917.
20. G. Tremiliosi-Filho, E. R. Gonzalez, A. J. Motheo, E. M. Belgsir, J.-M. Leger and C. Lamy, *J. Electroanal. Chem.*, 1998, **444**, 31-39.
21. B. N. Zope, D. D. Hibbitts, M. Neurock and R. J. Davis, *Science*, 2010, **330**, 74-78.
22. P. Rodriguez, Y. Kwon and M. T. M. Koper, *Nature Chem.*, 2012, **4**, 177-182.
23. C. E. M. Guarido, D. V. Cesar, M. M. V. M. Souza and M. Schmal, *Catal. Today*, 2009, **142**, 252-257.
24. J. P. Camplin and E. M. McCash, *Surf. Sci.*, 1996, **360**, 229-241.
25. X. Liu, B. Xu, J. Haubrich, R. J. Madix and C. M. Friend, *J. Am. Chem. Soc.*, 2009, **131**, 5757-5759.
26. Q. Meng, Y. Shen, J. Xu and J. Gong, *Chin. J. Catal.*, 2012, **33**, 407-415.
27. M. Boronat and A. Corma, *J. Catal.*, 2011, **284**, 138-147.
28. M. Boronat, A. Corma, F. Illas, J. Radilla, T. Ródenas and M. J. Sabater, *J. Catal.*, 2011, **278**, 50-58.
29. C. Shang and Z.-P. Liu, *J. Am. Chem. Soc.*, 2011, **133**, 9938-9947.
30. B. Xu, R. J. Madix and C. M. Friend, *J. Am. Chem. Soc.*, 2010, **132**, 16571-16580.
31. S.-C. Huang, C.-H. Lin and J. H. Wang, *J. Phys. Chem. C*, 2010, **114**, 9826-9834.
32. C.-H. Lin, C.-L. Chen and J.-H. Wang, *J. Phys. Chem. C*, 2011, **115**, 18582-18588.
33. Z.-P. Liu and P. Hu, *J. Am. Chem. Soc.*, 2003, **125**, 1958.
34. G.-C. Wang, S.-X. Tao and X.-H. Bu, *J. Catal.*, 2006, **244**, 10.
35. C.-Y. Syu and J.-H. Wang, *ChemCatChem*, 2013, **5**, 3164-3174.
36. I. X. Green, W. Tang, M. Neurock and J. T. Yates Jr., *Science*, 2011, **333**, 736-739.
37. S. Kandoi, A. A. Gokhale, L. C. Grabow, J. A. Dumesic and M. Mavrikakis, *Catal. Lett.*, 2004, **93**, 93-100.
38. T. Zhang, Z.-P. Liu, S. M. Driver, S. J. Pratt, S. J. Jenkins and D. A. King, *Phys. Rev. Lett.*, 2005, **95**, 266102.
39. H. Falsig, B. Hvolbæk, I. S. Kristensen, T. Jiang, T. Bligaard, C. H. Christensen and J. K. Nørskov, *Angew. Chem. Int. Ed.*, 2008, **47**, 4835-4839.
40. A. A. Herzing, C. J. Kiely, A. F. Carley, P. Landon and G. J. Hutchings, *Science*, 2008, **321**, 1331-1335.
41. J. A. Rodriguez, P. Liu, J. Hrbek, J. Evans and M. Perez, *Angew. Chem. Int. Ed.*, 2007, **46**, 1329.
42. A. A. Gokhale, J. Dumesic, A. and M. Mavrikakis, *J. Am. Chem. Soc.*, 2008, **130**, 1402-1414.
43. R. A. Ojifinni, N. S. Froemming, J. Gong, M. Pan, T. S. Kim, J. M. White, G. Henkelman and C. B. Mullins, *J. Am. Chem. Soc.*, 2008, **130**, 6801-6812.
44. R. Burch, *Phys. Chem. Chem. Phys.*, 2006, **8**, 5483.
45. C. Ratnasamy and J. P. Wagner, *Catal. Rev.*, 2009, **51**, 325.
46. G. Bond, *Gold Bull.*, 2009, **42**, 337.
47. V. Stamenkovic, B. S. Mun, K. J. J. Mayrhofer, P. N. Ross, N. M. Markovic, J. Rossmeisl, J. Greeley and J. K. Norskov, *Angew. Chem. Int. Ed.*, 2006, **45**, 2897.
48. Z. Yang, J. Li, X. Yang, X. Xie and Y. Wu, *J. Mol. Catal. A*, 2005, **241**, 15-22.
49. T. Yan, J. Gong and C. B. Mullins, *J. Am. Chem. Soc.*, 2009, **131**, 16189-16194.

50. P. B. Merrill and R. J. Madix, *Langmuir*, 1991, **7**, 3034-3040.
51. X. Liu and C. M. Friend, *Langmuir*, 2010, **26**, 16552-16557.
52. Y. Sugano, Y. Shiraishi, D. Tsukamoto, S. Ichikawa, S. Tanaka and T. Hirai, *Angew. Chem. Int. Ed.*, 2013, **52**, 5295-5299.
53. K.-i. Shimizu, K. Sugino, K. Sawabe and A. Satsuma, *Chem. Eur. J.*, 2009, **15**, 2341-2351.
54. C. D. Pina, E. Falletta and M. Rossi, *J. Catal.*, 2008, **260**, 384-386.
55. S.-X. Tao, G.-C. Wang and X.-H. Bu, *J. Phys. Chem. B*, 2006, **110**, 26045-26054.
56. B. K. Min, X. Deng, X. Liu, C. M. Friend and A. R. Alemozafar, *ChemCatChem*, 2009, **1**, 116-121.
57. M.-S. Liao and Q.-E. Zhang, *J. Mol. Catal. A*, 1998, **136**, 185-194.
58. R. Liu, W. Shen, J. Zhang and M. Li, *Appl. Surf. Sci.*, 2008, **254**, 5706-5710.
59. X.-Y. Pang, J.-J. Wang and G.-C. Wang, *J. Mol. Model*, 2012, **18**, 3793-3804.
60. G. Kresse and J. Hafner, *Phys. Rev. B*, 1993, **47**, 558-561.
61. G. Kresse and J. Hafner, *Phys. Rev. B*, 1994, **49**, 1425.
62. G. Kresse and J. Furthmüller, *Phys. Rev. B*, 1996, **54**, 11169-11186.
63. D. M. Cleperley and B. J. Alder, *Phys. Rev. Lett.*, 1980, **45**, 566.
64. J. P. Perdew and Y. Yang, *Phys. Rev. B*, 1992, **45**, 244.
65. P. E. Blöchl, *Phys. Rev. B*, 1994, **50**, 17953-17979.
66. G. Kresse and D. Joubert, *Phys. Rev. B*, 1999, **59**, 1758-1775.
67. H. J. Monkhorst and J. D. Pack, *Phys. Rev. B*, 1976, **13**, 5188-5192.
68. G. Mills, H. Jonsson and G. K. Schenter, *Surf. Sci.*, 1995, **324**, 305-337.

Table 1 Computed E_{ads} (eV) of CH_3CH_2OH*, CH_3CH_2O*, CH_3CHOH*, CH_3CHO*, H_2O*, OH*, O* and H* on the TM Surfaces.

	Co	Ni	Cu	Rh	Pd	Ag	Ir	Pt	Au
CH_3CH_2OH*	-0.30	-0.31	-0.21	-0.20	-0.27	-0.12	-0.25	-0.23	-0.09
CH_3CH_2O*	-2.91	-2.75	-2.50	-2.37	-1.88	-1.89	-2.04	-1.67	-1.33
CH_3CHOH*	-1.48	-1.49	-0.97	-1.69	-1.65	-0.55	-1.78	-1.95	-1.05
CH_3CHO*	-0.42	-0.39	-0.10	-0.49	-0.22	-0.07	-0.43	-0.19	-0.04
H_2O*	-0.35	-0.33	-0.26	-0.37	-0.30	-0.19	-0.39	-0.29	-0.12
OH*	-3.63	-3.40	-3.31	-3.08	-2.60	-2.75	-2.81	-2.32	-2.20
O*	-5.93	-5.68	-5.12	-5.40	-4.58	-3.90	-5.16	-4.52	-3.56
H*	-2.78	-2.76	-2.51	-2.86	-2.87	-2.09	-2.76	-2.78	-2.20

Table 2 Computed ΔE and *Ea* (eV) for the Four Steps in the Direct Dehydrogenation Reaction ($\mathbf{M_x}$) and Oxidative Dehydrogenation Reactions by O* ($\mathbf{O_x}$) and OH* ($\mathbf{OH_x}$) on the TM Surfaces, x Represents as **f1** and **f2** in the Frist Pathway and **s1** and **s2** in the Second Pathway.

			Co	Ni	Cu	Rh	Pd	Ag	Ir	Pt	Au
$\mathbf{M_{f1}}$	$CH_3CH_2OH^* + * \rightarrow CH_3CH_2O^* + H^*$	ΔE	-0.74	-0.58	-0.10	-0.19	0.25	0.84	0.21	0.55	1.00
		Ea	0.44	0.57	0.77	0.58	0.80	1.04	0.79	0.99	1.13
$\mathbf{M_{f2}}$	$CH_3CH_2O^* + * \rightarrow CH_3CHO^* + H^*$	ΔE	0.63	0.54	0.82	0.01	-0.18	0.67	-0.12	-0.18	0.06
		Ea	1.49	1.56	1.64	1.09	1.03	1.46	1.07	0.94	1.20
$\mathbf{M_{s1}}$	$CH_3CH_2OH^* + * \rightarrow CH_3CHOH^* + H^*$	ΔE	0.16	0.19	0.95	-0.03	-0.03	1.70	0.01	-0.21	1.08
		Ea	1.51	1.53	2.01	1.36	1.35	2.22	1.40	1.23	1.91
$\mathbf{M_{s2}}$	$CH_3CHOH^* + * \rightarrow CH_3CHO^* + H^*$	ΔE	-0.30	-0.35	-0.24	-0.13	-0.02	0.15	0.06	0.04	0.17
		Ea	0.66	0.64	0.72	0.76	0.87	0.95	0.82	0.82	0.95
$\mathbf{O_{f1}}$	$CH_3CH_2OH^* + O^* \rightarrow CH_3CH_2O^* + OH^*$	ΔE	0.01	0.01	-0.55	0.11	0.16	-0.46	0.15	0.01	-0.40
		Ea	0.62	0.65	0.19	0.69	0.62	0.13	0.66	0.53	0.25
$\mathbf{O_{f2}}$	$CH_3CH_2O^* + O^* \rightarrow CH_3CHO^* + OH^*$	ΔE	0.82	0.60	0.10	0.26	-0.28	-1.17	0.30	-0.28	-1.56
		Ea	1.30	1.20	1.05	1.08	0.94	0.66	1.04	0.86	0.57
$\mathbf{O_{s1}}$	$CH_3CH_2OH^* + O^* \rightarrow CH_2CHOH^* + OH^*$	ΔE	0.61	0.66	0.57	0.58	0.18	0.12	0.54	0.20	-0.06
		Ea	1.90	1.96	1.80	1.77	1.34	1.14	1.72	1.36	1.07
$\mathbf{O_{s2}}$	$CH_3CHOH^* + O^* \rightarrow CH_3CHO^* + OH^*$	ΔE	0.12	0.09	-0.68	0.15	-0.04	-1.58	0.44	0.41	-1.10
		Ea	0.45	0.43	0.14	0.49	0.43	0.02	0.50	0.58	0.09
$\mathbf{OH_{f1}}$	$CH_3CH_2OH^* + OH^* \rightarrow CH_3CH_2O^* + H_2O^*$	ΔE	0.16	0.16	-0.09	0.14	0.12	-0.19	0.07	0.08	-0.18
		Ea	0.48	0.59	0.18	0.46	0.47	0.08	0.47	0.41	0.05
$\mathbf{OH_{f2}}$	$CH_3CH_2O^* + OH^* \rightarrow CH_3CHO^* + H_2O^*$	ΔE	0.90	0.68	0.20	-0.40	-0.55	-1.06	-0.74	-0.87	-1.63
		Ea	1.08	0.96	0.82	0.62	0.58	0.49	0.65	0.56	0.37
$\mathbf{OH_{s1}}$	$CH_3CH_2OH^* + OH^* \rightarrow CH_2CHOH^* + H_2O^*$	ΔE	0.92	0.79	1.20	0.11	-0.16	0.95	-0.34	-0.44	0.11
		Ea	1.68	1.71	1.99	1.11	0.88	1.54	0.87	0.81	1.10
$\mathbf{OH_{s2}}$	$CH_3CHOH^* + OH^* \rightarrow CH_3CHO^* + H_2O^*$	ΔE	-0.10	-0.09	-0.88	-0.79	-0.83	-1.46	-0.96	-0.92	-1.52
		Ea	0.27	0.21	0.10	0.16	0.18	0.01	0.11	0.13	0.01

Figure captions

Fig. 1 (a) Energetic comparison of E_{ads} for CH_3CH_2OH*, CH_3CH_2O*, CH_3CHOH*, CH_3CHO*, H_2O*, OH*, O* and H* on the TM surfaces. (b) Optimized structures of CH_3CH_2OH*, CH_3CH_2O*, CH_3CHOH*, CH_3CHO*, H_2O*, OH*, O* and H* on Au(111). Yellow, grey, red and white spheres are represented as Au, C, O and H atoms.

Fig. 2. Optimized structures of the local minimums and transition states for the four steps in the direct dehydrogenation reaction and oxidative dehydrogenation reactions by O* and OH*, the steps listed in Table 2, on Au(111). Yellow, grey, red and white spheres are represented as Au, C, O and H atoms, respectively.

Fig. 3. (a) Energetic comparison of all *Ea* listed in Table 2: the 12 elementary steps on the nine TM surfaces. (b) (b) *Ea* differences between the oxidative and direct dehydrogenation reactions for step **f1**, [*Ea*(**O$_{f1}$**)–*Ea*(**M$_{f1}$**)] and [*Ea*(**OH$_{f1}$**)–*Ea*(**M$_{f1}$**)] in red and blue bars, respectively. (b) *Ea* differences between the oxidative and direct dehydrogenation reactions for step **f2**, [*Ea*(**O$_{f2}$**)–*Ea*(**M$_{f2}$**)] and [*Ea*(**OH$_{f2}$**)–*Ea*(**M$_{f2}$**)] in red and blue bars, respectively.

Fig. 4. (a) E_{ads} differences of [E_{ads}(OH*)–E_{ads}(O*)]–[E_{ads}(H*)] and [E_{ads}(H_2O*)–E_{ads}(OH*)]–[E_{ads}(H*)] on the TM surfaces in the adsorption/desorption energy analysis. (b) The energetic differences of [E_{bind}^{O*}(H) –E_{ads}(H*)] and [E_{bind}^{OH*}(H) –E_{ads}(H*)] on the TM surfaces in the binding energy analysis.

Fig. 5. DOS analysis for clean, O* and OH* adsorbed TMs. Metal d bands for bare, O* and OH* adsorbed surfaces are marked in solid, dot and dash blue lines, respectively. O atom p bands for $O_{(g)}$, $OH_{(g)}$, O* and OH* are marked in think solid, thin solid, dot and dash red lines, respectively.

Fig. 6. Induced charge rearrangement of O* on the TM surfaces in side and top views. Red and blue isosurfaces indicate depletion and addition of 0.03|e|/Å^3, respectively, referenced to the separated systems. TM atoms are marked in transparent yellow sphere.

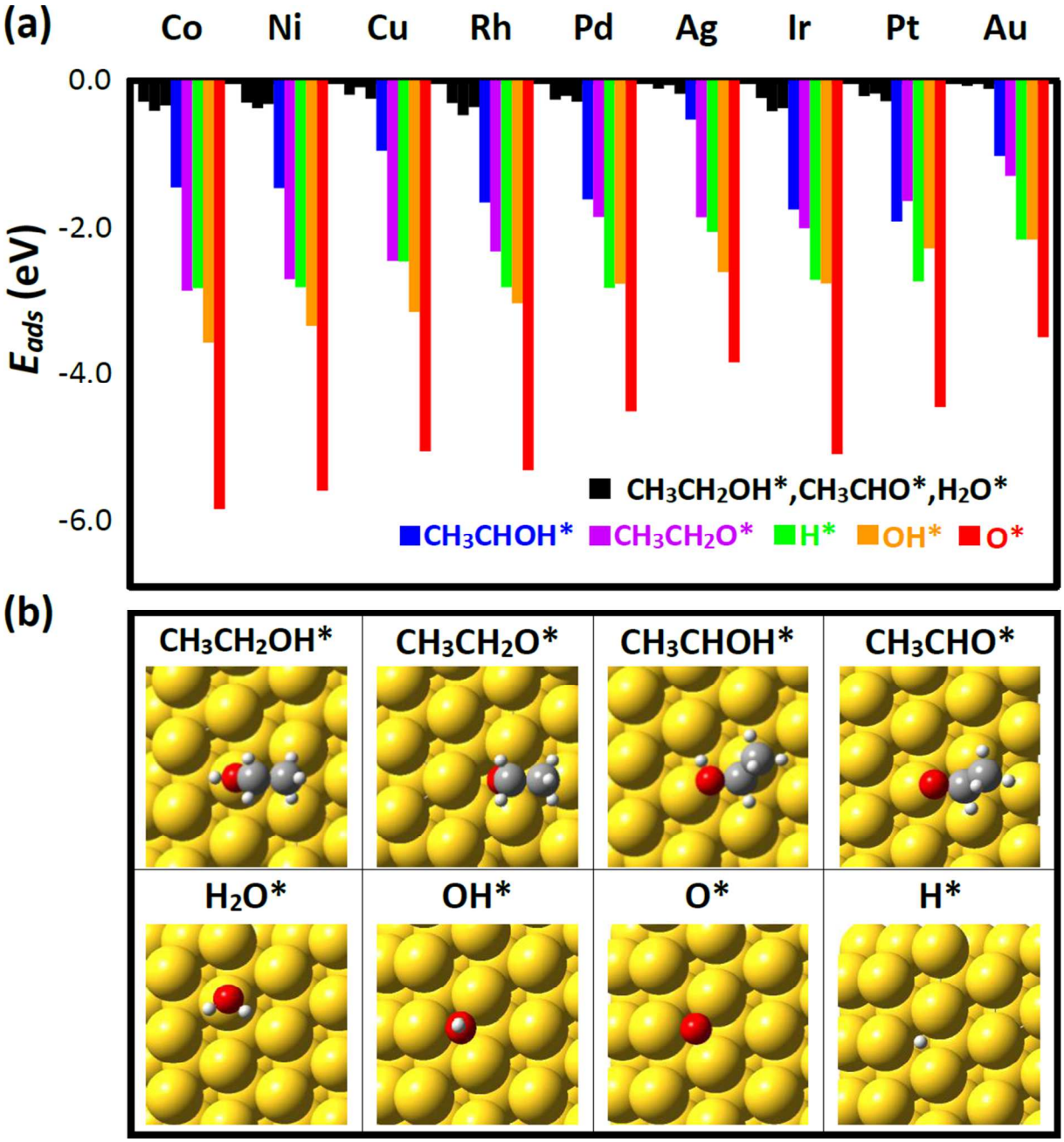

Fig. 1

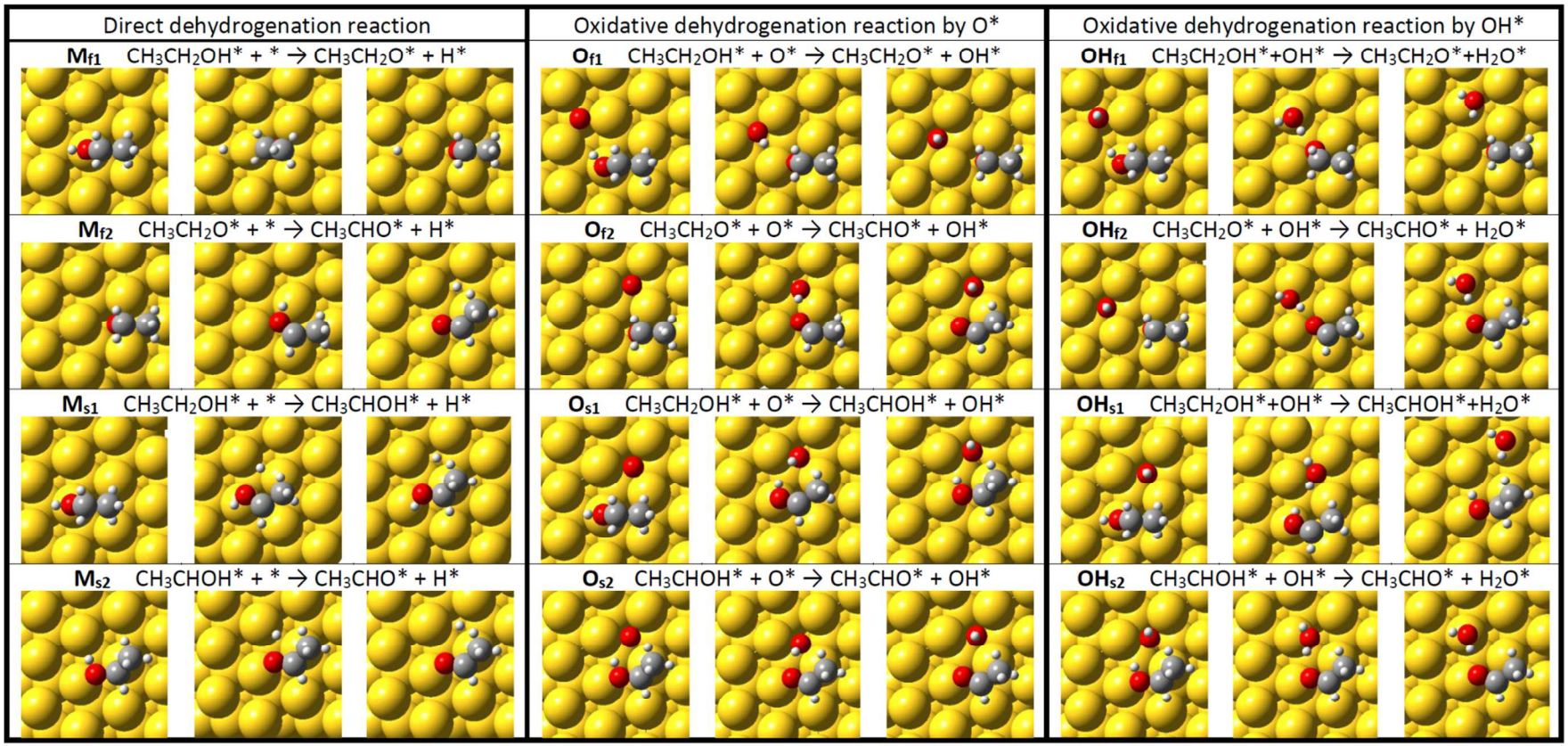

Fig. 2

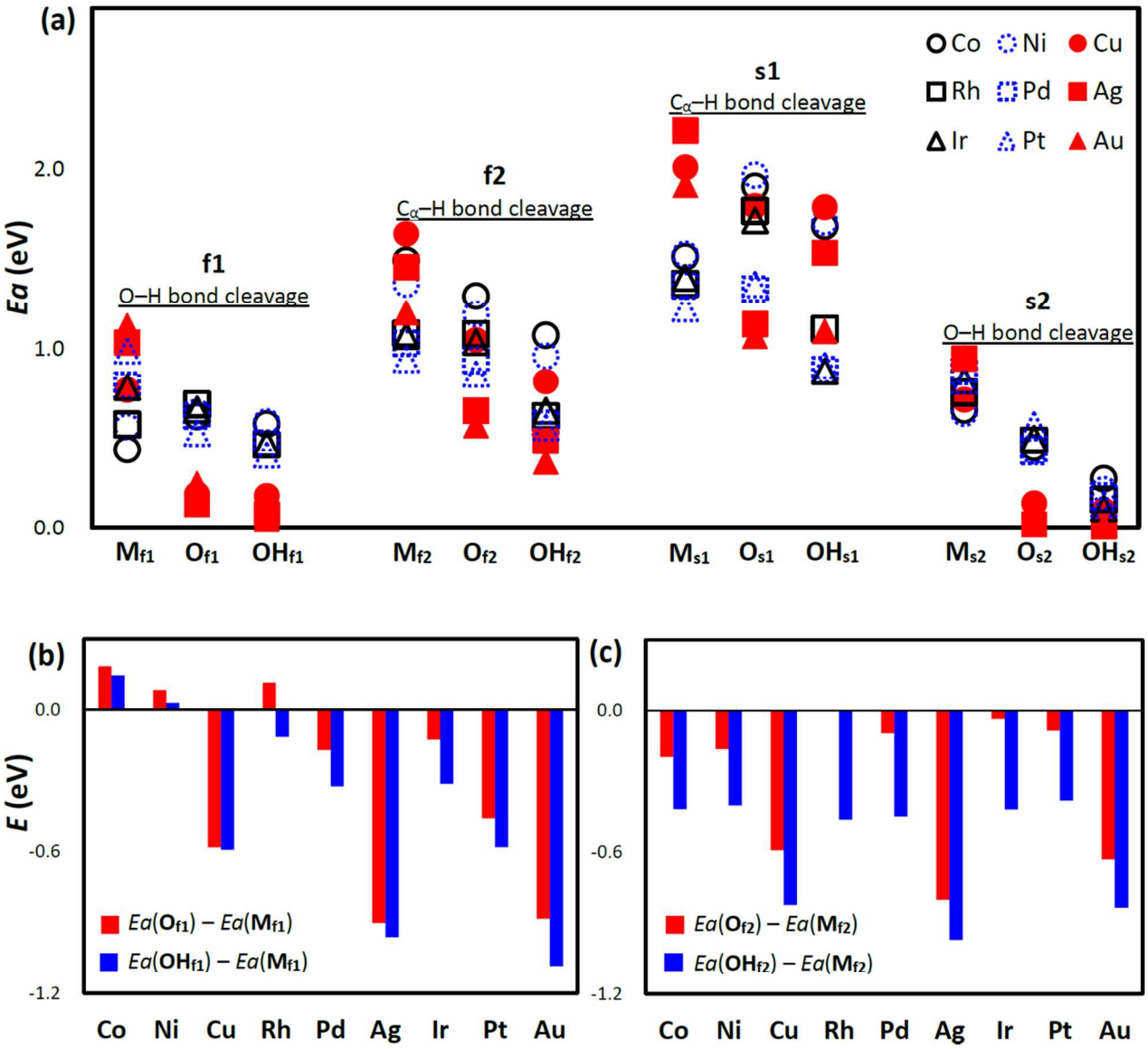

Fig. 3

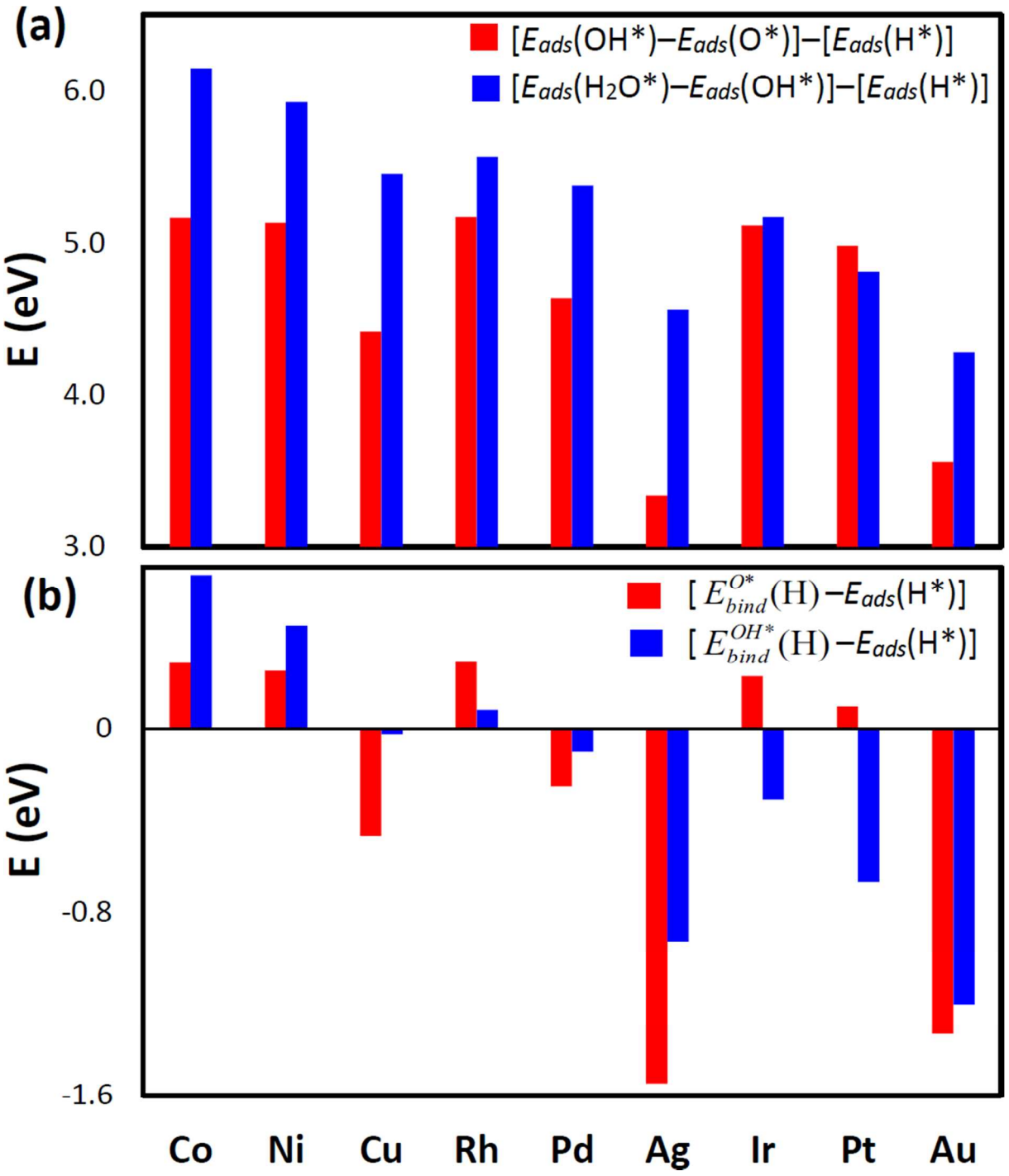

Fig. 4

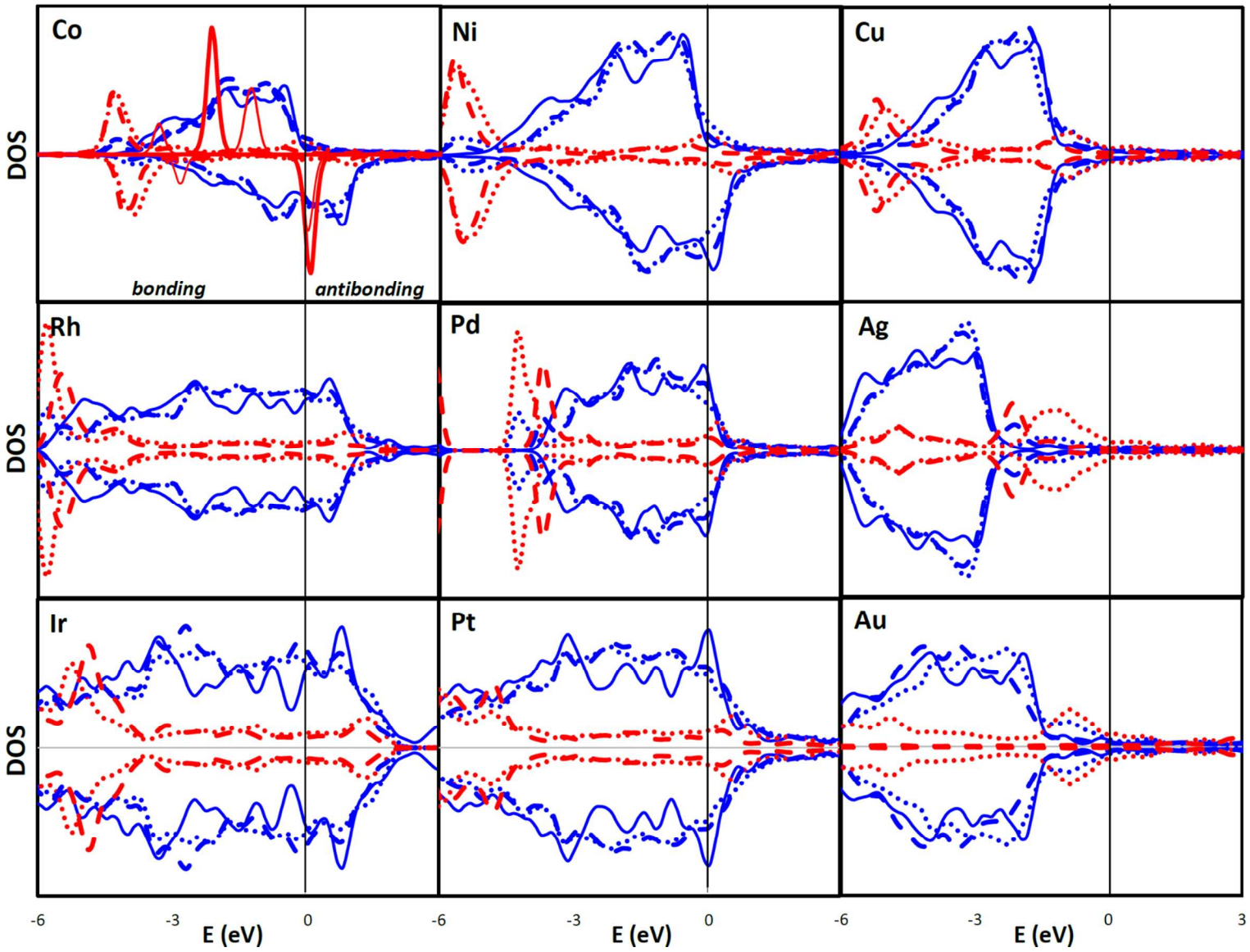

Fig. 5

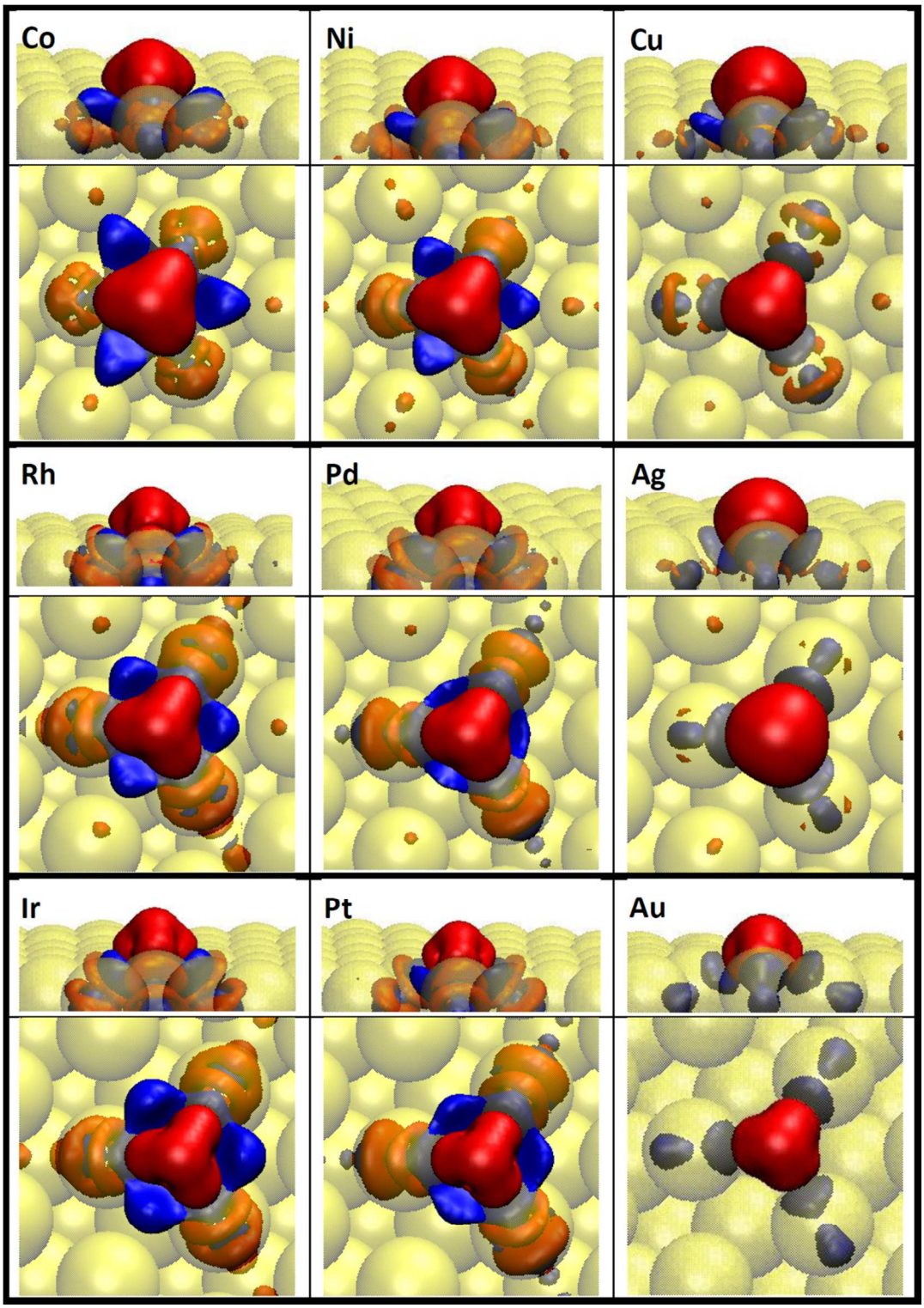

Fig. 6

A table of contents entry

Electronegative adspecies on inactive coinage metals can dramatically enhance the catalytic activity for oxidation as well as the dehydrogenation reactions.